


# The dynamic nature of $\alpha\text{TiO}_2$ : Implications for Ti-based thermometers in magmatic systems

**Journal Article****Author(s):**

Fonseca Teixeira, Ludmila Maria; [Troch, Juliana](#) ; Bachmann, Olivier

**Publication date:**

2024-01-01

**Permanent link:**

<https://doi.org/10.3929/ethz-b-000643070>

**Rights / license:**

[Creative Commons Attribution 4.0 International](#)

**Originally published in:**

Geology 52(1), <https://doi.org/10.1130/G51587.1>

**Funding acknowledgement:**

178928 - Dynamics of magma reservoirs in the earth's crust; focusing on the role of volatile elements (SNF)

# 1 **The dynamic nature of $a\text{TiO}_2$ : Implications for Ti-based** 2 **thermometers in magmatic systems**

3  
4 **L. M. Fonseca Teixeira<sup>1,2\*</sup>, J. Troch<sup>2</sup>, and O. Bachmann<sup>1</sup>**

5 <sup>1</sup> Department of Earth Sciences, ETH Zürich, 8092 Zürich, Switzerland

6 <sup>2</sup> Division of Earth Sciences and Geography, Faculty of Georesources and Materials, RWTH  
7 Aachen University, 52072 Aachen, Germany

8 \* ludmila.fonseca@erdw.ethz.ch

9  
10 <https://doi.org/10.1130/G51587.1>

11 Published online 20 November 2023

## 12 13 **ABSTRACT**

14 In recent decades, new Ti-based thermometers have found widespread use in  
15 geosciences, providing a convenient and powerful tool for investigating crystallization  
16 temperatures of quartz and zircons in magmatic systems. However, an often-overlooked  
17 aspect is the constraint of  $\text{TiO}_2$  activity ( $a\text{TiO}_2^{\text{liquid-rutile}}$ ). Many studies assume  $a\text{TiO}_2$  to be  
18 constant or equate the presence of Ti-rich phases, such as ilmenite, with fixed activity levels.  
19 Using solubility models and data from natural systems, we demonstrate that  $a\text{TiO}_2$  is a  
20 dynamic parameter, influenced by temperature, mineral assemblage, and  $\text{TiO}_2$  content in the  
21 melt. Focusing on examples from several volcanic fields (Bishop Tuff, Fish Canyon Tuff,  
22 Yellowstone, and Shiveluch), we discuss the impact of these factors on  $a\text{TiO}_2$  and highlight  
23 how inadequate constraint of  $a\text{TiO}_2$  can lead to erroneous interpretations of magma storage  
24 conditions.

25

## 26 INTRODUCTION

27 Temperature profoundly controls chemical systems by governing exsolution and  
28 solubility, and thus is critical for phase saturation, fluid exsolution, crystal structure and  
29 chemistry. In Earth sciences, accurately determining the temperatures of these processes, e.g.,  
30 through mineral-based thermometry, is essential for understanding the evolution of igneous,  
31 metamorphic, and hydrothermal systems. Titanium (Ti) thermometry finds extensive use in  
32 petrology, particularly for common phases like quartz (e.g. Wark and Watson, 2006; Huang  
33 and Audéat, 2012) and zircon ( e.g. Ferry and Watson, 2007; Loucks et al., 2020), known for  
34 their resistance to weathering and alteration. In situ Ti contents can be easily analyzed via  
35 laser-ablation-inductively coupled plasma-mass spectrometry (LA-ICP-MS) or electron probe  
36 microanalysis (EPMA).

37 All TiO<sub>2</sub>-based thermometers fundamentally hinge on constraining the titanium oxide  
38 activity in the melt from which minerals crystallize ( $a_{\text{TiO}_2}^{\text{liquid-rutile}}$ , [the TiO<sub>2</sub> activity in the  
39 melt with respect to rutile saturation] hereinafter  $a_{\text{TiO}_2}$ ).  $a_{\text{TiO}_2}$  is usually inferred from the  
40 presence of Ti-rich phases (e.g., rutile, ilmenite, Schiller and Finger, 2019), and assumed to be  
41 static. Small variations in  $a_{\text{TiO}_2}$  are typically deemed to have a minor impact on estimated  
42 temperatures.

43 In this paper, we discuss the underlying concepts of  $a_{\text{TiO}_2}$  and its substantial influence  
44 on the application of widely used thermometers. We argue that  $a_{\text{TiO}_2}$  is unlikely to remain  
45 constant in evolving magmatic systems and may exhibit significant temporal variations,  
46 underlining the importance of understanding the different methods to constrain  $a_{\text{TiO}_2}$ .  
47 Ultimately, a comprehensive and integrated approach considering multiple lines of evidence  
48 is necessary to establish and confidently utilize Ti-based geothermometers.

49

## 50 RUTILE SOLUBILITY MODELS

51 Solubility models based on experimental constraints help understand the behavior of  
52 Ti and  $a\text{TiO}_2$ . Models for Ti solubility were first developed by Hayden and Watson (2007)  
53 and later revised by Zhang et al. (2020), showing temperature (T) as a primary control of Ti  
54 solubility:

$$55 \log(Ti, ppm) = 6.5189 - \left(\frac{3006.5}{T(K)}\right) - 461 * \left(\frac{P^{0.2}}{T(K)}\right) + 0.1155 * FM \text{ (Eq. 1)}$$

56 Where P is pressure and FM is a compositional factor. The compositional factor FM is less  
57 relevant for comparisons within the same system, as it varies significantly only between  
58 different melts (e.g., FM varies from ~4 in basalts to 1.5 in rhyolites, Hayden and Watson,  
59 2007). Fractionation-induced variations in FM have negligible influence on Ti solubility since  
60 FM is multiplied by ~0.1, and melt compositions rarely span the entire range from basalt to  
61 rhyolite within the same system. Pressure variations (of more than several kilobars) affect  
62  $\text{TiO}_2$  solubility, but are unlikely within a given reservoir, making temperature the main  
63 varying factor.

64

65 In line with most solubility models, we consider  $a\text{TiO}_2$  in the melt relative to rutile  
66 saturation, i.e.  $a\text{TiO}_2 = 1$  when the system is rutile saturated. Thermodynamically,  $a\text{TiO}_2$  is  
67 calculated as:

$$68 a\text{TiO}_2^{\text{liquid-rutile}} = \frac{X\text{TiO}_2^{\text{liquid}} * \gamma\text{TiO}_2^{\text{liquid}}}{X\text{TiO}_2^{\text{liquid-saturated}} * \gamma\text{TiO}_2^{\text{liquid-saturated}}} \text{ (Eq. 2)}$$

69 Where  $X\text{TiO}_2$  is the  $\text{TiO}_2$  mole fraction in the melt, and  $\gamma\text{TiO}_2$  is the activity coefficient,  
70 influenced by melt composition, pressure and temperature (Borisov and Aranovich, 2020 –  
71 see the Supplemental Material).

72 It is evident that  $a\text{TiO}_2$  depends strongly on  $X\text{TiO}_2$  in the saturated melt, which  
73 according to the solubility equation, is primarily influenced by temperature. If the  $\text{TiO}_2$

74 content of the melt remains constant,  $a_{\text{TiO}_2}$  should increase as the system's temperature  
75 decreases (Fig. 1).

76

## 77 **MELT $\text{TiO}_2$ CONCENTRATIONS AND $a_{\text{TiO}_2}$ IN NATURAL SYSTEMS**

78 Evolving magmas may not maintain a constant  $\text{TiO}_2$  concentration in the melt.  $\text{TiO}_2$   
79 concentrations can either (1) increase due to precipitation of non-Ti-bearing minerals such as  
80 quartz and feldspar, resulting in the removal of other oxide components and the associated  
81 relative increase in  $\text{TiO}_2$  content (Fig. 2), or (2) decrease due to formation of Ti-bearing  
82 phases (e.g., rutile, ilmenite, titanite, or major minerals containing minor  $\text{TiO}_2$  such as  
83 pyroxenes and amphiboles). Consequently,  $a_{\text{TiO}_2}$  should not remain constant in an evolving  
84 magma reservoir.

85 By definition, a magma is at  $a_{\text{TiO}_2}^{\text{liquid-rutile}} = 1$  when rutile is present. However, rutile  
86 is almost never found in volcanic rocks, and rare in plutons. Hence,  $a_{\text{TiO}_2}$  must typically be  
87 lower than 1, and can be estimated by different techniques: (1) from co-crystallizing Fe-Ti  
88 oxides (Ghiorso and Gualda, 2013), providing  $a_{\text{TiO}_2}$  estimates over the temperature range of  
89 oxide crystallization, or (2) using thermodynamic software, such as MELTS or PerpleX  
90 (Connolly, 2005; Gualda et al., 2012). When both methods are applied to the same unit,  
91 results are not always consistent, e.g., in the Bishop Tuff, rhyolite-MELTS generally yields  
92 lower  $a_{\text{TiO}_2}$  than those from oxides (Fig. 2), despite being calibrated on this unit (Gualda et  
93 al., 2012). The inability of thermodynamic software to accurately predict saturation and  
94 composition of Fe-Ti oxides suggests that insufficient thermodynamic data currently hinders  
95 accurate determination of  $a_{\text{TiO}_2}$  through these programs.

96 When comparing multiple examples based on Fe-Ti oxides (Fig. 1), some systems  
97 exhibit increasing  $a_{\text{TiO}_2}$  with decreasing temperature, consistent with the expected down-  
98 temperature increase in  $\text{TiO}_2$  solubility. Others show the opposite, recording a down-

99 temperature decrease in  $a\text{TiO}_2$ , suggesting efficient  $\text{TiO}_2$  removal from the melt by Ti-bearing  
100 phases to compensate for the increase in  $a\text{TiO}_2$  resulting from cooling (Fig. 3). We used this  
101 data to model  $a\text{TiO}_2$  evolution in four natural systems (Bishop Tuff, California, western USA;  
102 Fish Canyon Tuff, Colorado, western USA; Shiveluch, Kamchatka, Russia; and Yellowstone,  
103 western USA; Fig. 1) as a function of different rates of  $\text{TiO}_2$  change with decreasing  
104 temperature ( $\partial\text{TiO}_2/\partial T$  in ppm/ $^\circ\text{C}$ ; see supplemental Material). More negative  $\partial\text{TiO}_2/\partial T$   
105 indicates greater fractionation of Ti phases and thus decrease of  $\text{TiO}_2$  with decreasing  
106 temperature. Two observations are noteworthy: (1) the trends in Fig. 1 cannot be fitted with  
107 constant  $\partial\text{TiO}_2/\partial T$ , but require that  $\partial\text{TiO}_2/\partial T$  varies with temperature, and (2) the contrasting  
108 trends in  $a\text{TiO}_2$  (e.g., Yellowstone and Shiveluch) occur over similar temperature and  
109  $\partial\text{TiO}_2/\partial T$  ranges, but are associated with high- $a\text{TiO}_2$  (Shiveluch) and low- $a\text{TiO}_2$  systems  
110 (Yellowstone). Our calculated values align with observations in these systems: for example,  
111 the hotter late-erupted Bishop Tuff, following a higher  $\partial\text{TiO}_2/\partial T$  trend, contains ~0.5% of  
112 ilmenite and titanomagnetite, while the early-erupted Bishop Tuff contains only ~0.05% of  
113 these Ti-bearing oxides (Hildreth, 1979).

114 Unlike high- $\text{TiO}_2$  systems near rutile-saturation, low- $\text{TiO}_2$  systems are very sensitive  
115 to crystallization of Ti-bearing phases, as even minor  $\text{TiO}_2$  removal can decrease  $a\text{TiO}_2$  (Fig.  
116 3). However,  $\text{TiO}_2$  removal from the melt through crystallization does not necessarily  
117 stabilize or decrease  $a\text{TiO}_2$  unless it occurs on a scale that compensates for the decreasing  
118 solubility and passive enrichment from non- $\text{TiO}_2$ -bearing phase crystallization. The  
119 logarithmic relationship between solubility and temperature suggests that  $a\text{TiO}_2$  in most  
120 magmas increases with decreasing temperature (Fig. 3), unless the crystallizing mineral  
121 assemblage decreases the  $\text{TiO}_2$  content by more than ~ 5 ppm/ $^\circ\text{C}$ .

122

123 **DO MINERALS BUFFER  $a\text{TiO}_2$  IN MAGMAS?**

124 Ilmenite has been suggested to crystallize at  $a\text{TiO}_2 \sim 0.5$  (Schiller and Finger, 2019)  
125 based on rhyolite-MELTS and PerpleX, and its presence is commonly used to constrain a  
126 system's  $a\text{TiO}_2$ . However, the presence of ilmenite in rutile-saturated rocks (e.g., Pikes Peak  
127 batholith, Colorado, Fonseca Teixeira et al., 2022) and experiments (Ryerson and Watson,  
128 1987) demonstrate that ilmenite can crystallize at much higher  $a\text{TiO}_2$  than 0.5. Co-existing  
129 Fe-Ti oxides indicate ilmenite precipitation at  $a\text{TiO}_2$  between 0.3 and 0.9 (Fig. 1), suggesting  
130 ilmenite saturation requires a minimum  $a\text{TiO}_2$  near 0.3 and can occur up to  $\text{TiO}_2$  saturation.  
131 Among the units with Fe-Ti oxide estimates (Fig. 1), none consistently exhibit  $a\text{TiO}_2 < 0.3$ .  
132 We suggest that extremely low values (e.g., 0.1) are unlikely near the solidus due to the  
133 temperature effect on solubility. A system starting at low  $\text{TiO}_2$  (e.g., 500 ppm at 1100°C,  
134 equivalent to  $a\text{TiO}_2 \sim 0.03$ ) would reach  $a\text{TiO}_2 = 0.6$  at the solidus (660°C, Fig. 1) through the  
135 temperature effect alone. The only way to reach  $a\text{TiO}_2$  as low as 0.1 near the solidus is  
136 through significant fractionation of  $\text{TiO}_2$ -bearing phases, which is unlikely at extremely low  
137  $a\text{TiO}_2$ . When disregarding the effect of Ti-free (or Ti-poor) silicate crystallization, only  
138 extremely  $\text{TiO}_2$ -poor melts (<100 ppm  $\text{TiO}_2$ ) could reach  $a\text{TiO}_2 \sim 0.1$  at 660 °C. We are not  
139 aware of any evolved igneous systems of such compositions.

140 Unlike rutile, ilmenite stability depends not only on  $a\text{TiO}_2$ , but also on other  
141 constituents, including oxygen fugacity, ferrous/ferric and Fe/Mg ratios (Frost, 1991),  
142 affecting the saturation and the mass of ilmenite crystallization. Hence, rocks with rutile do  
143 not necessarily contain ilmenite, and ilmenite presence cannot be used to assign a static  $a\text{TiO}_2$   
144 value.

145

#### 146 **ERRORS FROM FIXED $a\text{TiO}_2$**

147 Slightly over- or underestimating  $a\text{TiO}_2$  is often suggested to yield insignificant  
148 deviations from the true temperature (Fu et al., 2008). While this assumption can be valid, it

149 must be assessed carefully. Small discrepancies in  $a\text{TiO}_2$  are particularly relevant in low-  
150  $a\text{TiO}_2$  systems, e.g., at  $a\text{TiO}_2 = 0.9$  and 3 kbar, a quartz crystal with 50 ppm Ti yields 692 °C  
151 based on Huang and Audéat (2012). If  $a\text{TiO}_2$  is overestimated by 0.1, the same quartz gives a  
152 temperature of 705 °C (deviation of <15 °C). At lower  $a\text{TiO}_2$ , the same discrepancy in  $a\text{TiO}_2$   
153 leads to higher deviations, e.g., 60 °C difference for quartz with 50 ppm Ti at  $a\text{TiO}_2$  of 0.2  
154 and 0.3.

155         Temperature ranges of quartz crystallization (from saturation to low-T, interstitial  
156 quartz) are typically calculated assuming fixed  $a\text{TiO}_2$ . However, as discussed above,  $a\text{TiO}_2$  is  
157 unlikely to be constant unless the system is rutile-saturated, leading to significant  
158 discrepancies in Ti-in-quartz temperatures (Fig. 4). We compare Ti contents in quartz for a  
159 fixed  $a\text{TiO}_2$  of 0.5 and a dynamic  $a\text{TiO}_2$  value in the same system (Fig. 4 – see Suppl. Data  
160 for additional information). For a single point, the highest deviation (~100 °C) is at high-  
161  $a\text{TiO}_2$  (Shiveluch). However, the largest error in the estimated temperature range occurs for  
162 Bishop Tuff, where the range is ~100 °C larger at  $a\text{TiO}_2=0.5$  than with a dynamic  $a\text{TiO}_2$ ,  
163 leading to potential misinterpretations of the system's crystallization range. Furthermore, low-  
164 Ti quartz or zircon may be falsely interpreted as crystallized below the solidus (e.g.,  
165 temperatures as low as 620 °C for Yellowstone). For the Fish Canyon Tuff, Ti-in-quartz  
166 temperatures at dynamic  $a\text{TiO}_2$  are consistently 50 °C cooler, and are more consistent with  
167 quartz crystallization needing to be at lower temperatures than those measured by Fe-Ti  
168 oxides and amphibole-plagioclase thermometry immediately pre-eruption (~760 °C ; Whitney  
169 and Stormer, 1985; Johnson and Rutherford, 1989; Bachmann and Dungan, 2002) to explain  
170 the resorbed appearance of quartz in this unit (Bachmann et al., 2002).

171         Dynamic  $a\text{TiO}_2$  also affects the cathodoluminescence (CL) response of crystals and  
172 must be considered when interpreting CL images. Quartz with weak CL zoning might be  
173 interpreted as having formed over a narrow temperature range. However, if  $a\text{TiO}_2$  increases



174 sufficiently to compensate for the temperature decrease, quartz Ti contents vary minimally,  
175 resulting in weakly zoned crystals despite significant temperature variation. In summary,  
176 assuming a constant  $a\text{TiO}_2$  of 0.5 can lead to significant temperature discrepancies, and it is  
177 impossible to ascertain the scale of this effect without an accurate estimation of the  $a\text{TiO}_2$   
178 evolution.

179

## 180 **THE ROLE OF $a\text{TiO}_2$ IN THE BISHOP TUFF**

181         One of the main sources of controversy in studies on the Bishop Tuff is the origin of  
182 Ti-rich (80-100 ppm) rims in quartz crystals of the late-erupted Bishop Tuff, in abrupt contact  
183 to lower-Ti (40-50 ppm) cores (Peppard et al., 2001; Wark et al., 2007). Mafic recharge has  
184 been suggested to have induced the rim crystallization by elevating the temperatures and  
185 adding enough  $\text{CO}_2$  to allow quartz saturation at temperatures of  $\sim 800^\circ\text{C}$  (Wark et al., 2007).  
186 However, recharging the upper crustal magma reservoir with a less-differentiated, more Ti-  
187 rich melt would also affect Ti concentrations, e.g., mixing of early-erupted Bishop Tuff with  
188 5-13% of a Long Valley (California) andesite (Bailey, 1962) results in an increase of melt  
189  $\text{TiO}_2$  from  $\sim 0.07$  wt% to 0.12-0.19 wt%, comparable with late-erupted Bishop Tuff glass  
190 compositions (Suppl. Data). At a recharge mass fraction of  $\sim 13\%$ ,  $a\text{TiO}_2$  post-mixing would  
191 be at 0.8 at  $750^\circ\text{C}$ . A quartz with 100 ppm of Ti, at  $a\text{TiO}_2 = 0.8$  would crystallize at the same  
192  $\sim 750^\circ\text{C}$  (based on Huang and Audétat, 2012),  $50^\circ\text{C}$  lower than the temperatures originally  
193 calculated by Wark et al. (2007), and more compatible with experimental and modelled  
194 phased stabilities in the late-erupted Bishop Tuff (Gardner et al., 2014). Hence, only limited  
195 increase of temperature or addition of  $\text{CO}_2$  would be required to explain conditions recorded  
196 by the late-erupted Bishop Tuff: simply increasing the  $a\text{TiO}_2$  in the magma chamber to 0.8  
197 could explain crystallization of the high-Ti quartz rims (although such deeper, more mafic  
198 recharge would certainly add heat and  $\text{CO}_2$  to the system as well). Hence, we concur with

199 previous publications (e.g. Evans et al., 2016) that adding a small fraction of a less-  
200 differentiated melt from deeper in the system to the Bishop Tuff rhyolitic composition allows  
201 for the formation of high-Ti quartz rims . This highlights the role of  $a\text{TiO}_2$  regarding its most  
202 important parameters: temperature and  $\text{TiO}_2$  content in the melt.

203

## 204 CONCLUSIONS

205         Constraining  $a\text{TiO}_2$  in geological systems is a challenge, requiring careful  
206 consideration of various observations. Rutile reliably indicates  $\text{TiO}_2$  saturation. While it does  
207 not guarantee constant saturation throughout crystallization, substantial removal of  $\text{TiO}_2$  is  
208 needed to lower  $a\text{TiO}_2$  in rutile-saturated or near-saturated conditions. In rutile-undersaturated  
209 systems, ilmenite has traditionally been used to indicate  $a\text{TiO}_2 = 0.5$ , but this contradicts  
210 observations in natural and experimental samples. The presence of ilmenite suggests that  
211  $a\text{TiO}_2$  should be *at least* 0.3. Substantial precipitation of ilmenite and other Ti-bearing phases  
212 can lead to decreasing  $a\text{TiO}_2$  trends, counteracting the effect of cooling.

213         Further constraints can be derived from Ti concentrations in quartz and zircon. In  
214 quartz-saturated granitic systems close to haplogranite eutectic or minimum composition, the  
215 lowest Ti content of magmatic quartz (excluding dark-CL fluid inclusion trails and  
216 hydrothermal rims) can be approximated to solidus temperatures (650-680°C; Tuttle and  
217 Bowen, 1958; Luth et al., 1964; Piwinskii, 1968). Combining these observations not only  
218 allows us to estimate  $a\text{TiO}_2$  at the final stage of magmatic crystallization but also to infer  
219 potential evolution paths.

220         The overall Ti content also helps constrain probable  $a\text{TiO}_2$  values, e.g., Ti-rich quartz  
221 (>200 ppm) likely formed at high  $a\text{TiO}_2$  (>0.8). Similarly, zircon crystals with >30 ppm Ti  
222 likely precipitated at high  $a\text{TiO}_2$ . In contrast, low Ti quartz and zircons can mean low T  
223 and/or low  $a\text{TiO}_2$ . CL provides valuable insights, as abrupt changes signal events such as

224 recharge (Wark et al., 2007) and depressurization (Gualda and Ghiorso, 2013), that affect  
225 temperature,  $a_{\text{TiO}_2}$ , or both. In such cases,  $a_{\text{TiO}_2}$  should be considered separately for quartz  
226 and zircon before and after the change. For example, significant  $a_{\text{TiO}_2}$  increase following  
227 recharge and mixing may result in weak or even reverse Ti zoning in quartz (as seen in many  
228 volcanic systems). It is therefore essential to account for  $a_{\text{TiO}_2}$  variations in evolving  
229 magmatic systems to be able to recover meaningful temperatures from Ti-based mineral  
230 thermometers.

231

## 232 **ACKNOWLEDGMENTS**

233 This research was supported by Swiss SNF fund 200021\_178928 to Bachmann, and by the  
234 Grubermann-Burri Fund at ETHZ. We thank Rebecca Lange and two anonymous reviewers  
235 for feedback that helped clarify the discussion, and Andrew Barth for editorial handling.

236

## 237 **REFERENCES**

238

- 239 Bachmann, O., and Dungan, M.A., 2002, Temperature-induced Al-zoning in hornblendes of  
240 the Fish Canyon magma, Colorado: *American Mineralogist*, v. 87, p. 1062–1076,  
241 doi:10.2138/am-2002-8-903.
- 242 Bachmann, O., Dungan, M.A., and Lipman, P.W., 2002, The Fish Canyon Magma Body, San  
243 Juan Volcanic Field, Colorado: Rejuvenation and Eruption of an Upper-Crustal  
244 Batholith: *Journal of Petrology*, v. 43, p. 1469–1503,  
245 doi:10.1093/petrology/43.8.1469.
- 246 Bailey, R.A., 1962, *Eruptive History and Chemical Evolution of the Precaldera and*  
247 *Postcaldera Basalt-dacite Sequences, Long Valley, California: Implications for*  
248 *Magma Sources, Current Seismic Unrest, and Future Volcanism: U.S. Department of*  
249 *the Interior, U.S. Geological Survey*, 88 p.
- 250 Blundy, J., Cashman, K., and Humphreys, M., 2006, Magma heating by decompression-  
251 driven crystallization beneath andesite volcanoes: *Nature*, v. 443, p. 76–80,  
252 doi:10.1038/nature05100.
- 253 Borisov, A., and Aranovich, L., 2020, Rutile solubility and  $\text{TiO}_2$  activity in silicate melts: An  
254 experimental study: *Chemical Geology*, v. 556, p. 119817,  
255 doi:10.1016/j.chemgeo.2020.119817.

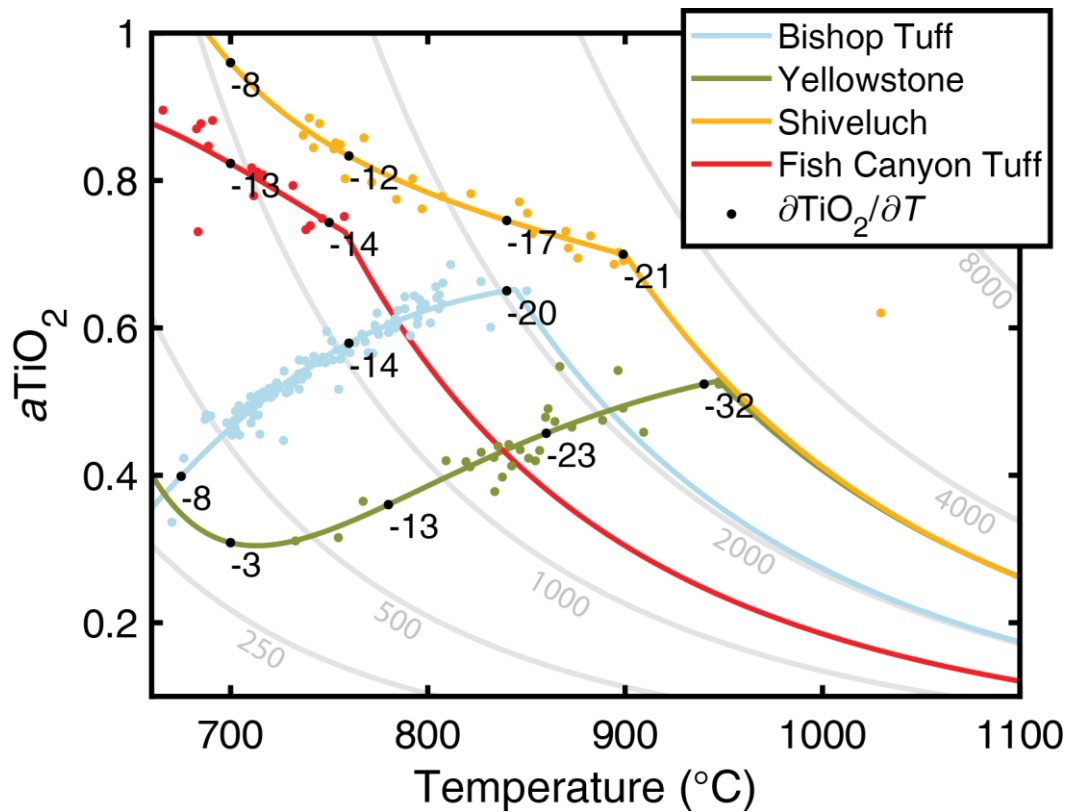
- 256 Cathey, H.E., and Nash, B.P., 2004, The Cougar Point Tuff: Implications for Thermochemical  
257 Zonation and Longevity of High-Temperature, Large-Volume Silicic Magmas of the  
258 Miocene Yellowstone Hotspot: *Journal of Petrology*, v. 45, p. 27–58,  
259 doi:10.1093/petrology/egg081.
- 260 Connolly, J.A.D., 2005, Computation of phase equilibria by linear programming: A tool for  
261 geodynamic modeling and its application to subduction zone decarbonation: *Earth and  
262 Planetary Science Letters*, v. 236, p. 524–541, doi:10.1016/j.epsl.2005.04.033.
- 263 Evans, B.W., Hildreth, W., Bachmann, O., and Scaillet, B., 2016, In defense of magnetite-  
264 ilmenite thermometry in the Bishop Tuff and its implication for gradients in silicic  
265 magma reservoirs: *American Mineralogist*, v. 101, p. 469–482, doi:10.2138/am-2016-  
266 5367.
- 267 Ferry, J.M., and Watson, E.B., 2007, New thermodynamic models and revised calibrations for  
268 the Ti-in-zircon and Zr-in-rutile thermometers: *Contributions to Mineralogy and  
269 Petrology*, v. 154, p. 429–437, doi:10.1007/s00410-007-0201-0.
- 270 Fonseca Teixeira, L.M., Troch, J., Allaz, J., and Bachmann, O., 2022, Magmatic to  
271 hydrothermal conditions in the transition from the A-type Pikes Peak granite  
272 (Colorado) to its related pegmatite: *Frontiers in Earth Science*, v. 10,  
273 <https://www.frontiersin.org/articles/10.3389/feart.2022.976588> (accessed July 2023).
- 274 Frost, B.R., 1991, Introduction to oxygen fugacity and its petrologic importance, *in* *Oxide  
275 minerals*, Donald H. Lindsley, Berlin, De Gruyter, p. 1–10.
- 276 Fu, B., Page, F.Z., Cavosie, A.J., Fournelle, J., Kita, N.T., Lackey, J.S., Wilde, S.A., and  
277 Valley, J.W., 2008, Ti-in-zircon thermometry: applications and limitations:  
278 *Contributions to Mineralogy and Petrology*, v. 156, p. 197–215, doi:10.1007/s00410-  
279 008-0281-5.
- 280 Gardner, J.E., Befus, K.S., Gualda, G.A.R., and Ghiorso, M.S., 2014, Experimental  
281 constraints on rhyolite-MELTS and the Late Bishop Tuff magma body: *Contributions  
282 to Mineralogy and Petrology*, v. 168, p. 1051, doi:10.1007/s00410-014-1051-1.
- 283 Ghiorso, M.S., and Gualda, G.A.R., 2013, A method for estimating the activity of titania in  
284 magmatic liquids from the compositions of coexisting rhombohedral and cubic iron-  
285 titanium oxides: *Contributions to Mineralogy and Petrology*, v. 165, p. 73–81,  
286 doi:10.1007/s00410-012-0792-y.
- 287 Gualda, G.A.R., and Ghiorso, M.S., 2015, MELTS\_Excel: A Microsoft Excel-based MELTS  
288 interface for research and teaching of magma properties and evolution: *Geochemistry,  
289 Geophysics, Geosystems*, v. 16, p. 315–324, doi:10.1002/2014GC005545.
- 290 Gualda, G.A.R., and Ghiorso, M.S., 2013, The Bishop Tuff giant magma body: an alternative  
291 to the Standard Model: *Contributions to Mineralogy and Petrology*, v. 166, p. 755–  
292 775, doi:10.1007/s00410-013-0901-6.
- 293 Gualda, G.A.R., Ghiorso, M.S., Lemons, R.V., and Carley, T.L., 2012, Rhyolite-MELTS: a  
294 Modified Calibration of MELTS Optimized for Silica-rich, Fluid-bearing Magmatic  
295 Systems: *Journal of Petrology*, v. 53, p. 875–890, doi:10.1093/petrology/egr080.

- 296 Harrison, T.M., Watson, E.B., and Aikman, A.B., 2007, Temperature spectra of zircon  
297 crystallization in plutonic rocks: *Geology*, v. 35, p. 635, doi:10.1130/G23505A.1.
- 298 Hayden, L.A., and Watson, E.B., 2007, Rutile saturation in hydrous siliceous melts and its  
299 bearing on Ti-thermometry of quartz and zircon: *Earth and Planetary Science Letters*,  
300 v. 258, p. 561–568, doi:10.1016/j.epsl.2007.04.020.
- 301 Hildreth, W., 1981, Gradients in silicic magma chambers: Implications for lithospheric  
302 magmatism: *Journal of Geophysical Research: Solid Earth*, v. 86, p. 10153–10192,  
303 doi:10.1029/JB086iB11p10153.
- 304 Hildreth, W., 1979, The Bishop Tuff: evidence for the origin of compositional zonation in  
305 silicic magma chambers, in Chapin, C.E., and Elston, W.E., eds., *Ash-Flow Tuffs*:  
306 *Geological Society of America Special Paper*, v. 180, p. 43–75.
- 307 Hildreth, E.W., 1977, The magma chamber of the Bishop Tuff: Gradients in Temperature,  
308 Pressure, and Composition: University of California, Berkeley.
- 309 Huang, R., and Audétat, A., 2012, The titanium-in-quartz (TitaniQ) thermobarometer: A  
310 critical examination and re-calibration: *Geochimica et Cosmochimica Acta*, v. 84, p.  
311 75–89, doi:10.1016/j.gca.2012.01.009.
- 312 Johnson, M.C., and Rutherford, M.J., 1989, Experimental calibration of the aluminum-in-  
313 hornblende geobarometer with application to Long Valley caldera (California)  
314 volcanic rocks: *Geology*, v. 17, p. 837–841, doi:10.1130/0091-  
315 7613(1989)017<0837:ECOTAI>2.3.CO;2.
- 316 Loucks, R.R., Fiorentini, M.L., and Henríquez, G.J., 2020, New Magmatic Oxybarometer  
317 Using Trace Elements in Zircon: *Journal of Petrology*, v. 61, p. egaa034,  
318 doi:10.1093/petrology/egaa034.
- 319 Luth, W.C., Jahns, R.H., and Tuttle, O.F., 1964, The granite system at pressures of 4 to 10  
320 kilobars: *Journal of Geophysical Research (1896-1977)*, v. 69, p. 759–773,  
321 doi:10.1029/JZ069i004p00759.
- 322 Osborne, Z.R., Thomas, J.B., Nachlas, W.O., Angel, R.J., Hoff, C.M., and Watson, E.B.,  
323 2022, TitaniQ revisited: expanded and improved Ti-in-quartz solubility model for  
324 thermobarometry: *Contributions to Mineralogy and Petrology*, v. 177, p. 31,  
325 doi:10.1007/s00410-022-01896-8.
- 326 Peppard, B.T., Steele, I.M., Davis, A.M., Wallace, P.J., and Anderson, A.T., 2001, Zoned  
327 quartz phenocrysts from the rhyolitic Bishop Tuff: *American Mineralogist*, v. 86, p.  
328 1034–1052, doi:10.2138/am-2001-8-910.
- 329 Piwinski, A.J., 1968, Experimental Studies of Igneous Rock Series Central Sierra Nevada  
330 Batholith, California: *The Journal of Geology*, v. 76, p. 548–570, doi:10.1086/627359.
- 331 Ryerson, F.J., and Watson, E.B., 1987, Rutile saturation in magmas: implications for TiNbTa  
332 depletion in island-arc basalts: *Earth and Planetary Science Letters*, v. 86, p. 225–239,  
333 doi:10.1016/0012-821X(87)90223-8.

- 334 Schiller, D., and Finger, F., 2019, Application of Ti-in-zircon thermometry to granite studies:  
335 problems and possible solutions: *Contributions to Mineralogy and Petrology*, v. 174,  
336 p. 51, doi:10.1007/s00410-019-1585-3.
- 337 Thomas, J.B., Bruce Watson, E., Spear, F.S., Shemella, P.T., Nayak, S.K., and Lanzirotti, A.,  
338 2010, TitaniQ under pressure: the effect of pressure and temperature on the solubility  
339 of Ti in quartz: *Contributions to Mineralogy and Petrology*, v. 160, p. 743–759,  
340 doi:10.1007/s00410-010-0505-3.
- 341 Troch, J., Ellis, B.S., Harris, C., Bachmann, O., and Bindeman, I.N., 2020, Low- $\delta^{18}\text{O}$  silicic  
342 magmas on Earth: A review: *Earth-Science Reviews*, v. 208, p. 103299,  
343 doi:10.1016/j.earscirev.2020.103299.
- 344 Tuttle, O.F., and Bowen, N.L., 1958, Origin of granite in the light of experimental studies in  
345 the system  $\text{NaAlSi}_3\text{O}_8\text{--KAlSi}_3\text{O}_8\text{--SiO}_2\text{--H}_2\text{O}$ , in Tuttle, O.F. and Bowen, N.L. eds.,  
346 *Origin of Granite in the Light of Experimental Studies in the System NaAlSi}\_3\text{O}\_8\text{--}*  
347 *KAlSi}\_3\text{O}\_8\text{--SiO}\_2\text{--H}\_2\text{O}, Geological Society of America, v. 74, p. 0,  
348 doi:10.1130/MEM74-p1.*
- 349 Wark, D.A., Hildreth, W., Spear, F.S., Cherniak, D.J., and Watson, E.B., 2007, Pre-eruption  
350 recharge of the Bishop magma system: *Geology*, v. 35, p. 235–238,  
351 doi:10.1130/G23316A.1.
- 352 Wark, D.A., and Watson, E.B., 2006, TitaniQ: a titanium-in-quartz geothermometer:  
353 *Contributions to Mineralogy and Petrology*, v. 152, p. 743–754, doi:10.1007/s00410-  
354 006-0132-1.
- 355 Whitney, J.A., and Stormer, J.C., JR., 1985, Mineralogy, Petrology, and Magmatic Conditions  
356 from the Fish Canyon Tuff, Central San Juan Volcanic Field, Colorado: *Journal of*  
357 *Petrology*, v. 26, p. 726–762, doi:10.1093/petrology/26.3.726.
- 358 Zhang, C., Li, X., Almeev, R.R., Horn, I., Behrens, H., and Holtz, F., 2020, Ti-in-quartz  
359 thermobarometry and  $\text{TiO}_2$  solubility in rhyolitic melts: New experiments and  
360 parametrization: *Earth and Planetary Science Letters*, v. 538, p. 116213,  
361 doi:10.1016/j.epsl.2020.116213.

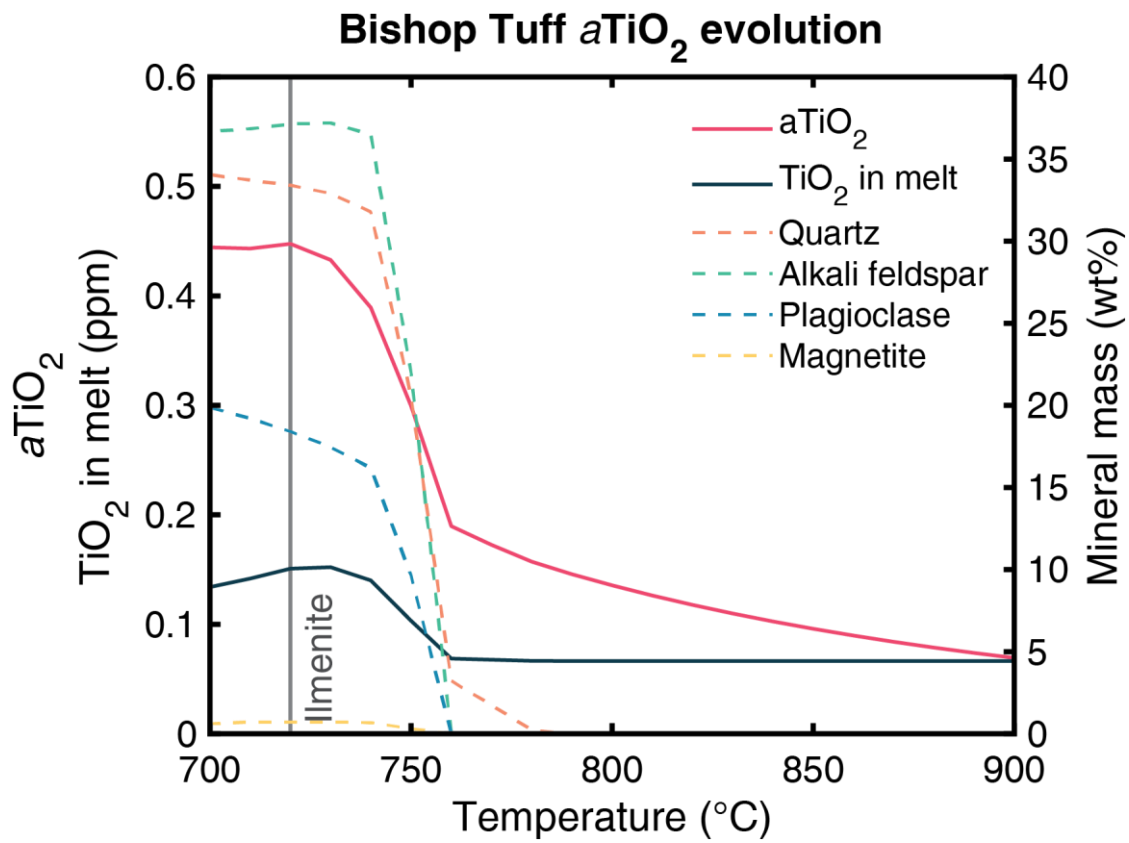
362

363 **FIGURES**



364

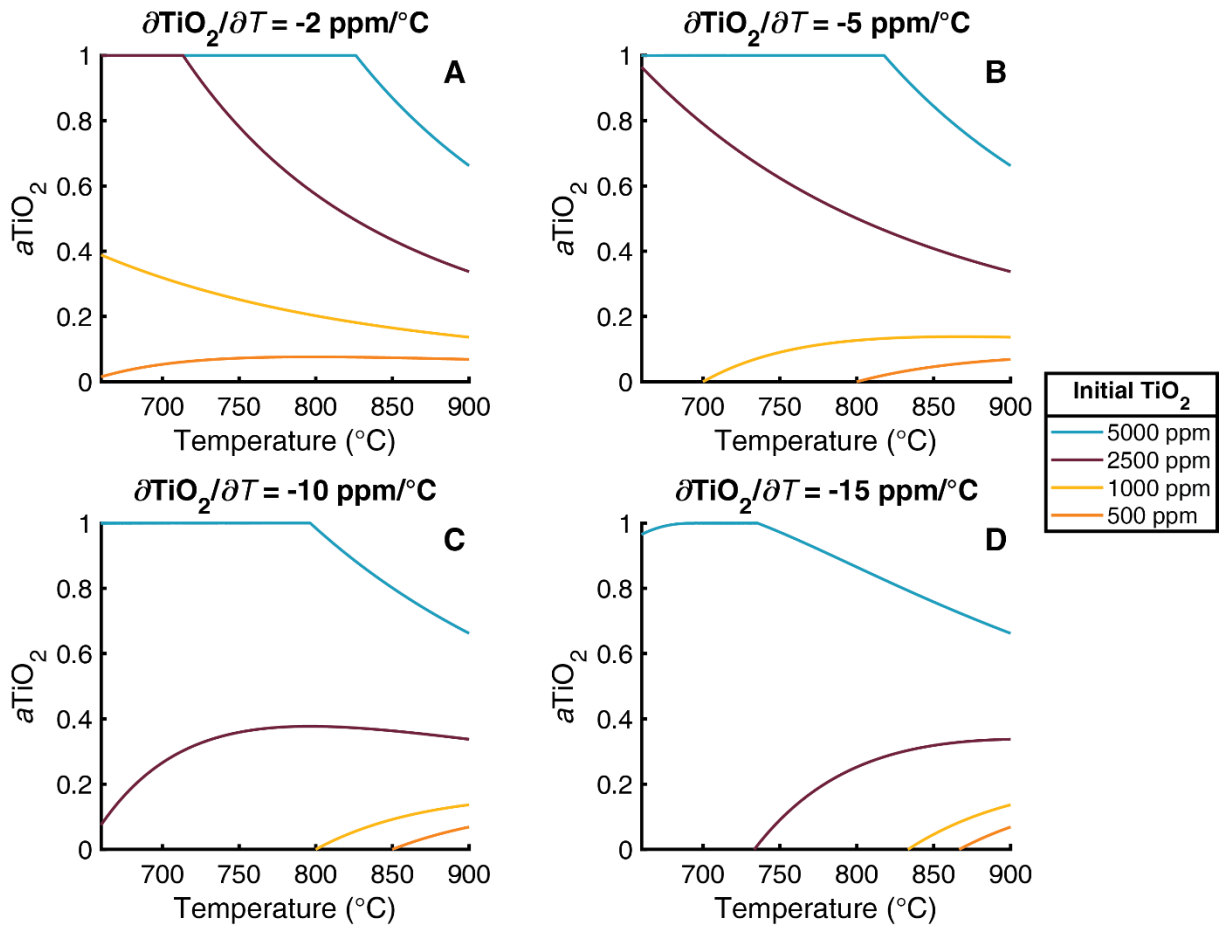
365 Fig. 1:  $\text{TiO}_2$  activity ( $a\text{TiO}_2$ ) in natural systems from co-existing magnetite-ilmenite pairs  
 366 (Ghiorso and Gualda, 2013): Bishop Tuff (California, USA; full sequence, Hildreth, 1977),  
 367 Yellowstone (western United States; Lava Creek and Huckleberry Ridge Tuffs, Hildreth,  
 368 1981, Cougar Point Tuff, Cathey and Nash, 2004), Shiveluch (Kamchatka, Russia; 2001-2004  
 369 eruptions, Blundy et al., 2006), and Fish Canyon Tuff (Colorado, USA; outflow sheet,  
 370 Whitney and Stormer, 1985). Grey lines mark solubility relationships in melts with constant  
 371  $\text{TiO}_2$  (in ppm). Colored lines mark best-fit  $a\text{TiO}_2$ -temperature (T) relationships as function of  
 372 variable  $\partial\text{TiO}_2/\partial T$  (variation in ppm  $\text{TiO}_2$  per  $1^{\circ}\text{C}$  decrease); black numbers show  $\partial\text{TiO}_2/\partial T$   
 373 along this trend.



374

375 Fig. 2: Left axis:  $a\text{TiO}_2$  and  $\text{TiO}_2$  in the Early Bishop Tuff calculated with MELTS for Excel  
 376 (Gualda and Ghiorso, 2015). Right axis: mass of crystallized phases. The vertical line marks  
 377 the start of ilmenite precipitation.



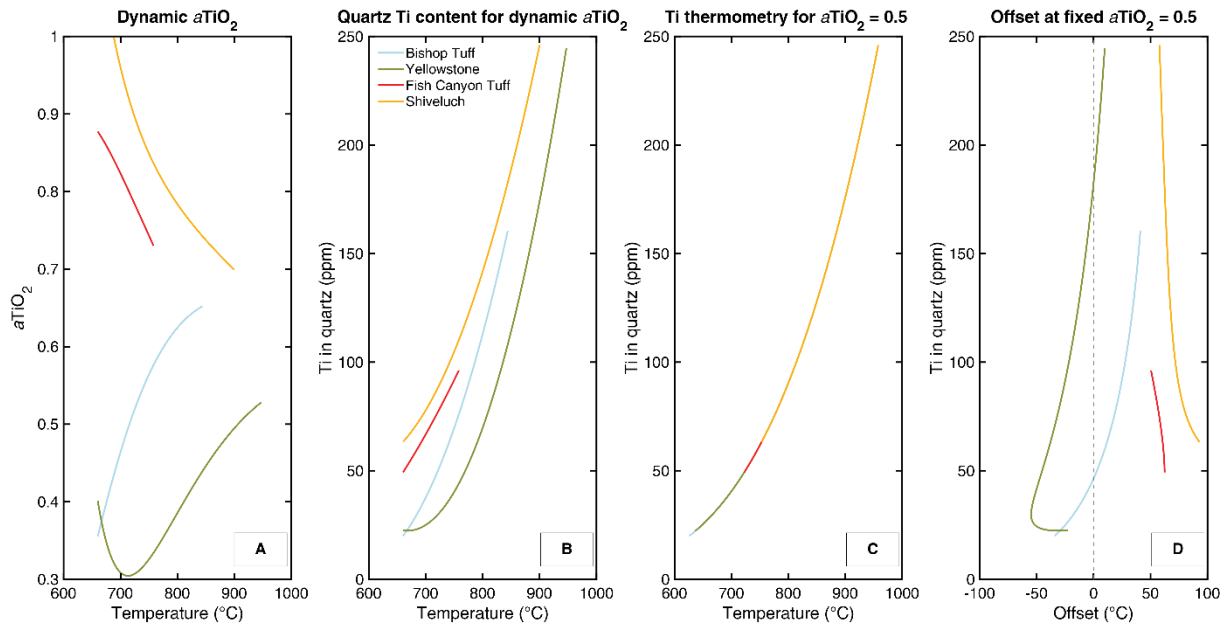


378

379 Fig. 3:  $a_{\text{TiO}_2}$  evolution for melts with different initial  $\text{TiO}_2$  contents at different  $\partial\text{TiO}_2/\partial T$   
 380 calculated for an average Yellowstone-Heise composition (Troch et al., 2020) and calculating  
 381  $a_{\text{TiO}_2}$  with the method from (Borisov and Aranovich, 2020).

382

383



384

385 Fig. 4: (A)  $a\text{TiO}_2$  evolution for examples from Fig. 1. (B) Hypothetical Ti content in quartz  
 386 co-crystallizing with Fe-Ti oxides, based on Huang and Audetat (2012) and  $a\text{TiO}_2$  activities  
 387 in (A). (C) Ti-in-quartz thermometry for fixed  $a\text{TiO}_2 = 0.5$ . Note how all lines from B  
 388 collapse into a single trend. (D) Temperature offset between dynamic and fixed  $a\text{TiO}_2$ .